3D failure of a scale-down dry stone retaining wall: a DEM modelling

Quezada, J., Vincens, E., Mouterde, R., Morel, J.

Original citation & hyperlink:
Quezada, J-C, Vincens, E, Mouterde, R & Morel, J-C 2016, '3D failure of a scale-down dry stone retaining wall: a DEM modelling' Engineering Structures, vol 117, pp. 506-517. DOI: 10.1016/j.engstruct.2016.03.020
https://dx.doi.org/10.1016/j.engstruct.2016.03.020

DOI 10.1016/j.engstruct.2016.03.020
ISSN 0141-0296

Publisher: Elsevier

3D failure of a scale-down dry stone retaining wall: a DEM modelling

Juan-Carlos Quezada[a], Eric Vincens[a,*], Rémy Mouterde[b], Jean-Claude Morel[c]

[a]University of Lyon, LTDS, UMR CNRS 5513, École centrale de Lyon, Écully, France
[b]Laboratory of Shape Analysis, Ecole Nationale Supérieure d'Architecture de Lyon, Vaulx en Velin Cedex, France.
[c]Coventry University, Faculty of Engineering, Environment and Computing, School of Energy, Construction and Environment, Centre for Low Impact Buildings, Priory Street, CV1 5FB, United Kingdom.

Abstract

Dry stone retaining walls are vernacular structures that can be found in many places around the world and were mainly built to reduce slope erosion and to allow agricultural practices. Their stability is essentially warranted by the global wall weight and the capacity of individual blocks to develop friction at contact. The arrangement of these hand-placed blocks contributes also to the stability of the wall. A new interest arose in these structures in the last years, first due to the necessity to repair damages inherent to any built heritage, but also to their possible advantages regarding sustainability.
Several studies have tried to address the behavior of slope dry stone retaining walls, whereas few conclusive studies have been performed concerning road dry stone retaining walls. In this latter case, the loading implies, apart from the backfill, the existence of a concentrated force on the backfill surface. The failure of such masonry work is accompanied by true three-dimensional deformations.
This study is a first attempt to provide a better understanding of the mechanical behavior of road dry stone retaining walls. It involves a small-scale prototype with clay bricks for the wall, and steel blocks, acting as a concentrated loading on the backfill surface at a given distance from the inward wall face. Steel blocks have been superposed until wall failure. A numerical study based on these experiments is then performed by means of a mixed discrete-continuum approach.
The numerical model was able to retrieve the average value of the concentrated force triggering failure found in the experiences, except when the concentrated loading is very close to the wall. Nevertheless, the results provided by this study are considered as encouraging even if further work is required to definitely state about the validity of such a numerical technique for the study of actual road dry stone retaining walls.

Keywords: Dry stone, retaining walls, DEM, small-scale test

1. Introduction

Dry stone retaining walls (DSRWs) are structures composed of individual hand-placed blocks of stone without mortar where stability is primarily obtained by the global weight of the wall and the existing friction at block contacts. Nevertheless, the specific arrangement of blocks, creating a three dimensional meshing, also contributes to the wall stiffness and stability. The organization of the assembly of blocks may vary according to regional traditions and the environmental context, especially in presence of strong water flows, for example in the case of structures built across thalwegs or on seafront.

This kind of structure can be found in many places around the world where suitable material is available. A large number of these structures have been raised up until the beginning of the 20th century, when this constructive method was replaced by modern techniques, such as reinforced concrete [1]. However, in recent decades, a new interest has arisen in dry stone retaining walls, mainly for the necessary maintenance and repair of this former damaged built heritage.

The behavior of these structures is quite specific: they are able to experiment large deformations before failure, dissipating large amounts of energy by friction among blocks. In this sense, their behavior is different from reinforced concrete structures. The other specificity lies in the absence of an existing regulation for the design and the repairing of dry stone retaining walls and local administrations that manage roads and highways are helpless in front of this ageing retaining wall stock.

Despite these drawbacks, this technology seems appealing since it addresses some concerns of the sustainable development. Indeed, DSRWs are generally made of local primary materials, require few embodied energy for their construction and at the end-of-life time, the stone blocks can be re-used for repairing the wall or can be used for new masonry constructions.

In order to evaluate the performances of these peculiar masonry structures, several studies have been conducted in the

*Corresponding author. Tel.: +33 4 72 18 62 21.
Email address: eric.vincens@ec-lyon.fr (Eric Vincens)

past using both experimental and numerical approaches.

The first known basic study on these structures was performed by Burgoyne [2] who built in Kingstown four DSRWs of granite with different geometries in order to identify the best one to support the backfill pressure. Later, full-scale tests were conducted by Villemus et al. [3] to study the plane-strain failure of plane slope DSRWs. In that work, the wall failure was reached by applying a hydrostatic loading on the inward wall face. Colas et al. [4] also studied the plane strain failure of slope DSRWs by gradually dumping a non-cohesive material as backfill up to the wall collapse. Finally, Mundell et al. [5] performed full-scale experiments where they analyzed the typical bulged wall profile generated at bottom wall. To achieve this profile, they used an external localized force applied directly on the backfill while imposing a settlement to the wall foundation.

In the literature, numerical modelings of the DSRWs behavior are based on the finite element method (FEM) [6] or on a discrete element method (DEM) in order to keep the discrete nature of the wall composed of individual blocks. This latter method can take into account the specific arrangement of the blocks and can get a better local insight of these retaining structures. Harkness [7] modeled Burgoyne's field experiments using UDEC code (DEM, ITASCA code) [8], confirming the qualitative results Burgoyne obtained. Also based on Burgoyne's tests, Powrie et al. [9] and later Claxton et al. [10], performed numerical simulations, studying the influence of the mechanical properties and geometry of blocks on the wall stability. Recently, Oetomo et al. [11] modeled the behavior of slope DSRWs by two methods. The first technique involved a fully DEM approach where both the wall and the backfill grains were modeled as individual bodies. The second method was based on a mixed discrete-continuum approach where the wall was modeled using individual blocks while the backfill was modeled by a continuum approach. The software PFC2D and UDEC (ITASCA codes) were used for the fully discrete approach and the mixed discrete-continuum approach respectively. The objective of these works was to retrieve the critical loading heights observed through full-scale experiments performed by Villemus et al. [3] and Colas et al. [4]. All these before-mentioned studies showed the capability of DEM to retrieve the mechanical behavior of slope DSRWs.

Nevertheless, these studies are mainly based on 2D models and are related to plane slope retaining walls. In this case, failure takes place following a plane strain mode, which is not the case of road retaining walls.

In this work, the case of road retaining walls is studied. For this kind of walls, failure occurs with a 3D state of deformations and a 3D modeling is then required. The aim is therefore to validate the use of a 3D mixed discrete-continuum approach to study the behavior of road DSRWs. This study is just a preliminary step where simulations of small-scale experiments involving an idealized road DSRW have been carried out. However, in the future, further validations that will be based on full-scale experiments and involving irregular stone blocks will be required to definitively state about the ability of this numerical approach to accurately model the behavior of actual road DSRWs.

In the first part of this work, the small-scale experiment is presented together with the different cases of loadings. The walls were loaded by a concentrated loading placed on the backfill until reaching the wall collapse. Then, the numerical model is described and the technical points related to the modeling of the whole system are addressed. Finally, the results from numerical and experimental tests are compared to validate the proposed numerical model.

2. Small-scale experiments

2.1. Set up

The physical model is composed of a box that is filled in by a backfill composed of sand. A wall made of clay bricks which are idealized models for actual stone blocks is loaded by this backfill. The box is 110cm width, 50cm depth and 40cm height (Fig.1a). The depth and length are large enough to prevent any side effects on the wall failure that is studied. The brick wall is of 88cm width (lengthwise), 3.3cm thick and 16cm height. This wall is made of bricks with individual dimensions: 33mm, 16mm and 11mm height (Fig.1b and Fig.1c).

For the small-scale model, an arrangement of blocks formed by a header and two blocks in stretcher was chosen (Fig.1b and Fig.1c). Despite the random nature of stone block shapes in actual DSRWs, this block organization seems to be a fundamental element of these structures. As it can be seen in Fig.1b and Fig.1c, for the stability of the wall, the outward movement of the first row of bricks was restrained by a fixed wood plate. The lengthwise lateral extremes of the wall are prevented from moving in the X-axis direction, and only partly according to the Y-axis. It will be shown that this latter imperfection has a negligible influence on the failure of the brick wall.

2.2. Loading of the wall

First, a backfill is installed which is a first loading stage of the wall. The backfill material is a Hostun sand (D_{50} = 0.37mm, D_{10} = 0.2mm, CU=1.9, e_{min} = 0.648, e_{max} = 1.041 [12]).The relative density R_D of the material measured in the experiments is equal to 2% and corresponds to a measured bulk density of 1300 kg.m^{-3} and a void ratio of 1.032. The material is then in a very loose state.

The material is dry and was uniformly pluviated in the box at a zero drop height from the ground surface of the backfill. The pouring is stopped when the backfill surface level reaches the wall head. Finally, approximately 114kg of sand have been

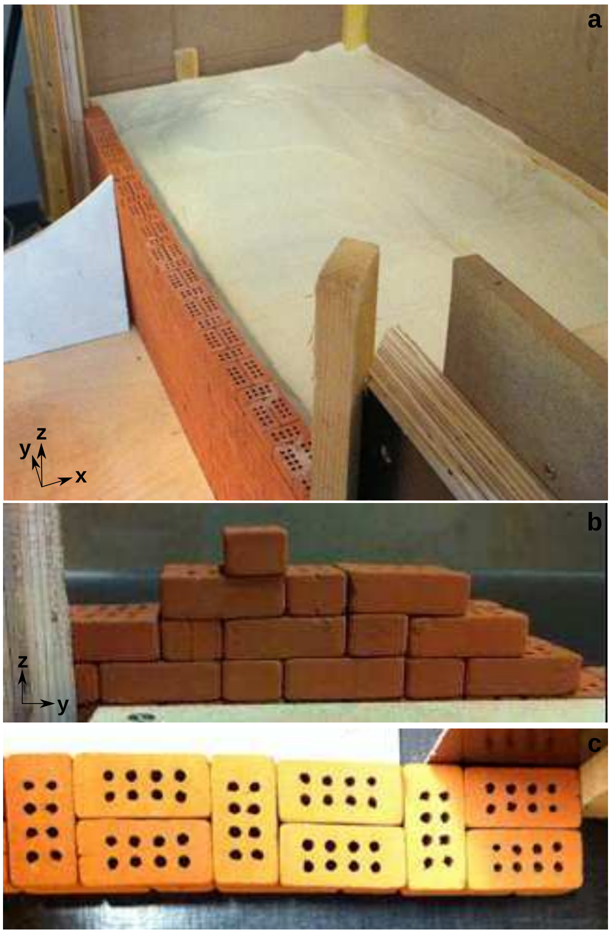

Figure 1: a) Box for the experimental set-up. Focus on the arrangement of bricks within the wall: b) Frontal plane view; c) Horizontal plane view.

installed.

Secondly, a concentrated loading is applied on the backfill surface by means of superposed steel blocks of 6cm by 7cm width. Different distances d between the block and the inward wall face were investigated: 2cm, 3cm and 4cm. This concentrated loading is expected to model the impact of a vehicle traveling on a road and located at the top retaining wall, in a simple manner. The technique that consists to transform dynamic forces into equivalent static forces is typical of structural approaches involved in road and bridge design codes (e.g. Eurocode 1). Herein, just the static vertical action coming from the contact surface between the wheel and the road is modeled.

A first steel block is placed in the backfill, 1cm under its surface in order to improve the block stability during the loading process. A level is used to warranty that the top face of this block is inclined within one degree of horizontal (Fig.2). Then, subsequent blocks of 2kg, 1kg, 0,5kg or 0,1kg are superposed on this first block until wall failure. Herein, failure is defined as the total collapse of the wall.

Figure 2: Loading process in the experimental set-up.

Because the creation of the wall and the sand deposit are both sets of a random process, different experiments were performed considering any distance d between the steel block and the inward wall face. More precisely, five different tests were performed for each value of d. For a given value of d, a first test is performed and an estimate for the maximum concentrated loading triggering failure is obtained by successively superposing steel blocks of 0.5kg ($\simeq$ 5N) on the backfill. This value is considered as just indicative and will be rejected as a definite result. Then, five tests are performed with a better precision using steel blocks of 0.1kg ($\simeq$ 1N) when approaching the former identified failure.

In Fig.3, we give for each distance d the mean value for this maximum force together with the associated error bar, i.e. the minimum and maximal value obtained in the five experiments.

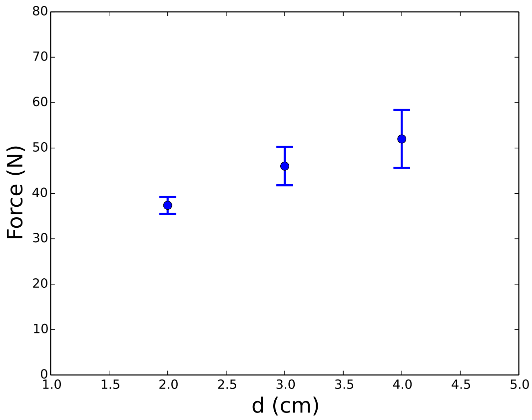

Figure 3: Maximum load applied at failure for each distance d between the steel block and the inward wall face. Error bars take into account the minimum and maximum observed loads in the experiments.

The experimental results show a variability which increases with d. This feature is mainly due to the transfer of stresses within the backfill material. For d = 2cm, the transfer of the concentrated loading towards the wall does not involve the

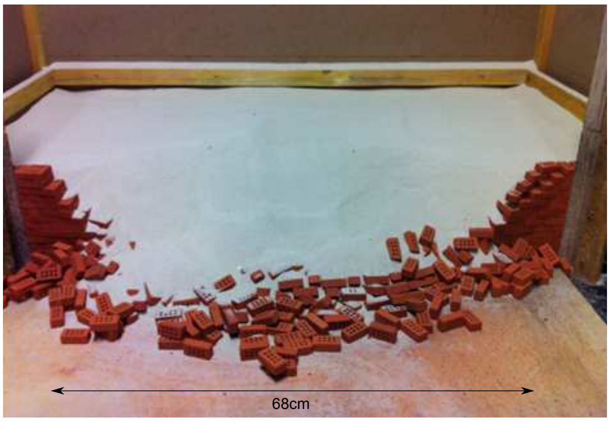

Figure 4: View of the experimental setup-up after failure, d = 4cm.

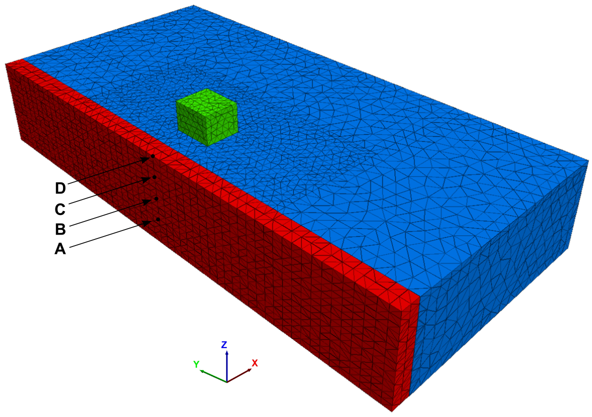

Figure 5: Sketch of the numerical model; points A, B, C, D are measurement points.

same sand volume as in the case of $d = 4$cm which is far larger in this latter case. Any heterogeneity within the backfill, which is more likely to be found in the latter case, is expected to disturb the way the concentrated loading is transferred to the wall. As a result, a broader variation of the maximum concentrated loading is expected too for $d = 4$cm.

Finally, we show in Fig.4 the typical wall state after failure (collapse) for d equal to 4cm, case where the extent of the concentrated loading influence on the wall is maximum. One can note that failure does not affect the lateral sides of the wall which tends to prove that the length of the brick wall is large enough to prevent any boundary effects on the failure process.

3. Numerical modeling

A numerical modeling based on the experiments presented in section 2 was carried out using the software 3DEC (ITASCA code).

3.1. Basic aspects about 3DEC

This software is based on an explicit solution method for the solvation of the equations of the dynamics and can model discontinuities in a material by the discrete element method. The system is then modeled by an assembly of polyhedra where relative displacements and rotations are allowed between them. These blocks can be either rigid or deformable and, in this instance, the deformability of the blocks is handled by means of the finite difference method. Consequently, 3DEC allows geotechnical or construction problems to be solved by a mixed discrete-continuum approach [13]. In the past, this code was used to get more insight into the behavior of plane DSRWs where pathologies observed on site and the behavior of specific DSRWs toward failure could have been reproduced [7, 9, 10, 14].

The particularity of DEM codes is related to the existence of a contact law between the bodies in interaction. In this work, the so-called joint between bricks is ruled by a Coulomb-slip model. Each joint is discretized into sub-contacts, created at the vertices of the brick face, where interaction forces are applied. In the linear elastic domain, the behavior of the sub-contacts is ruled by a unique normal and a shear stiffness (K_n and K_s respectively). The increments in relative displacement for a sub-contact of the joint are used to calculate the elastic force increments. The incremental law for the normal force F_n is written:

$$\Delta F_n = -K_n \Delta U_n A_c \tag{1}$$

where ΔU_n is the incremental normal relative displacement of the sub-contact of the joint and A_c is the area of the sub-contact. For a component i of the shear force increment vector ΔF_s, the law is written:

$$\Delta F_i^s = -K_s \Delta U_i^s A_c \tag{2}$$

where ΔU_i^s is the component i of the incremental tangential relative displacement vector. A maximum shear force is allowed for a sub-contact and is given by a generalized Coulomb law:

$$F_{\max}^s = C A_c + F_n \tan\phi \tag{3}$$

where C and ϕ are the cohesion and the friction angle of the joint respectively. The incremental tangential relative displacement can generate a dilation and in this case, the normal force is corrected to account for the effect of dilation.

3.2. Description of the numerical model

In this work, the wall is made of individual deformable bodies with deformable contacts and the backfill material is considered as a continuum medium. A joint is added between the wall blocks, which is also the case between the wall blocks and the backfill.

First, to create the wall, a large block is built including the total geometry of the wall. Then, this object is cut with

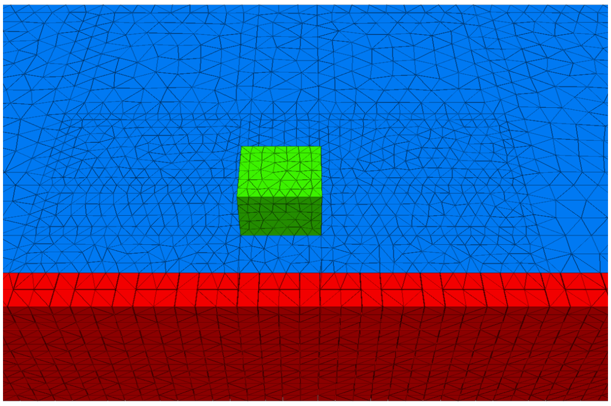

Figure 6: Focus on the refined mesh zone.

horizontal and vertical planes to form brick shapes according to the arrangement described in section 2. Then, the backfill is created in a single stage. The loading block is placed inside an excavation created into the backfill surface with depth 1cm to conform the experimental process. Finally, the entire system is meshed. This mesh is composed of tetrahedral elements generated by a Delaunay partition of the whole space (Fig.5).

A refinement of the meshing is performed in a zone of 45cm length and 20cm width, centered on the loading block, in order to obtain accurate calculations with the finite difference method (Fig. 6). This zone encompasses the entire height of the backfill. For a general case, it was checked that the chosen mesh refinement allows us to obtain a stabilized computation where the result is no more influenced by the mesh size. The refinement must be nevertheless limited to a value that allows the computation to be carried out. Indeed, strong deviatoric deformations are generally created below the steel block and an excessive refinement facilitates the concentration of these deformations. Then, the capacity of the finite difference method to deal with these very distorted meshes gives a upper bound to the refinement of the mesh.

The mesh size for the wall blocks is uniform and chosen in relation to the smallest mesh size of the backfill (hence from the refined zone). Finally, a block is composed of eight elements. It ensures a correct transfer of information between the backfill and the wall by the wall-backfill joint. For example, in the refined zone, there are on the average six gridpoints from the backfill in contact with a wall block through the joint (Fig. 6).

Concerning the wall boundary conditions, the first row of bricks are fixed like in the experiments and the lateral sides of the retaining walls are just allowed to move vertically. In the experimental set-up, the sand at the backfill boundaries is in contact with the walls of the box. In the numerical model, the associated gridpoints on the external vertical faces are only allowed to move vertically, while at the backfill base, the gridpoints can only move horizontally.

To follow the movement of the wall towards failure, four points belonging to the outward wall face were chosen and were monitored throughout the simulations (Figure 5). They belong to the cross-sectional plane of symmetry of the entire system. They are denoted point A, B, C and D with a respective altitude of $H/4$, $H/2$, $3H/4$ and H, H being the total height of the wall. Point D is then a point at wall head.

3.3. Constitutive laws and model parameters

The mechanical problem of DSRWs is based on three mechanical sub-systems that must be correctly identified and consequently characterized: the wall, the backfill and the wall-backfill interface.

The bulk density of the bricks was found equal to 1635 kg.m^{-3}. The behavior of the bricks is expected to follow a Hooke law. The elastic parameters were taken from the literature with a shear modulus G equal to 4.17×10^{8}Pa and a bulk modulus K equal to 5.56×10^{8}Pa.

The contact law of the joint between two bricks is elastic which requires the definition of both a normal and tangential stiffness (Eq.1 and Eq.2). In this work, for the sake of simplicity, the tangential stiffness is taken equal to the normal stiffness. They are both set to 1×10^{9}Pa.m^{-1} [7, 11]. These stiffnesses do not hold a true physical meaning which is a typical approach in DEM. They are generally large enough not to disturb the quality of the results while not to excessively penalize computation times as well. The cohesion for the joint is equal to zero since the joint is dry (Eq. 3). The friction angle at contact between the bricks was experimentally identified using an inclined plane test involving two superposed squared-layers of eight bricks each one, with 83mm length side, following the same brick arrangement as in the wall. The brick-to-brick friction angle was found equal to $32° \pm 2°$. The dilatancy angle is set to zero. Indeed, very little dilatancy was observed during the test on the inclined plane.

For the backfill, an elastic/plastic Mohr-Coulomb constitutive model was chosen. This model is the typical model used in geotechnical engineering when only little information about the behavior of the soil is available. Moreover, the use of a more sophisticated constitutive model is beyond our capacity to identify the model parameters. Indeed, most of the data available for Hostun sand and able to allow model parameters to be calibrated come from tests performed for a confinement greater than 50kPa which is far beyond the average pressure involved in these scale-down experiments (0.7kPa at wall mid-height). The average Young modulus E for the sand was identified using the general formula proposed by Biarez and Hicher [15] $E = \frac{450}{e}\sqrt{p'}$ where e is the void ratio and p' the average effective pressure in MPa. A value of 11.5MPa was found but for the sake of simplicity, a Young modulus of 10MPa was preferred in this study. Nevertheless, further

Property	wall bricks	backfill	interface
ρ (kg.m^{-3})	1635	1300	-
K (Pa)	5.56×10^8	8.33×10^6	-
G (Pa)	4.17×10^8	3.85×10^6	-
ϕ (°)	32	32	20
Ψ (°)	0	0	0
Cohesion C (kPa)	0	0	0
K_n (Pa.m^{-1})	1×10^9	-	1×10^9
K_s (Pa.m^{-1})	1×10^9	-	1×10^9

Table 1: Mechanical properties used in the numerical simulations for the wall bricks, the backfill and the backfill-wall interface.

results will also be provided for a Young modulus of 5MPa and 15MPa, which is a possible range of values for this property in this study. Indeed, one must understand that the formula by Biarez and Hicher [15] was derived from tests performed with confining pressures greater than 100kPa and its validity can be questioned for the range of confining pressures involved in this work. Moreover, from isotropic compression tests on sands, some authors found that the dependency of the elastic properties of granular materials with respect to the confining pressure may involve a multiplicative power different from 0.5 (which is the case for Biarez and Hicher's formula), typically ranging between 0.4 and 0.6 [16, 17]. In this work, for the sake of simplicity, and due to the lack of information on the dependency of the Young modulus with respect to pressure in the range of stresses involved in the experiments, the backfill shear modulus is supposed to be constant and independent on depth. Moreover, a too small value of the Young modulus close to the surface would create excessively deformable layers that would lead to unrealistic settlements under the steel blocks when loading. The Poisson ratio is taken equal to 0.3.

The other mechanical properties of the backfill are those of a very loose sand. It means that the internal friction angle of the sand is equal to its critical state angle. Flavigny et al. [12] performed various triaxial tests on Hostun sand with a confining pressure of 50kPa. They found a critical state angle of 32° for this sand. In the literature, there are no existing triaxial tests for confinements smaller than 50kPa which is far larger than the representative average pressure herein in the backfill (0.7kPa). Nevertheless, the angle of repose for Hostun sand which is close to the critical state angle was identified. Two tests have been carried out where a slope was created while by pouring the material on the top of the slope with a quasi-zero drop height. Different measurements were performed along the slope for the two tests and an angle of repose of 31.8° ±0.5° was identified. Consequently, the tests tends to validate the value found by Flavigny et al. [12] which can be used even for confining stresses smaller than 50kPa. Thus, an internal friction angle of 32° is used in this study for Hostun sand. Finally, considering the very loose state of the backfill material, the dilation angle Ψ for the granular material is set to zero. Cohesion is equal to zero for this purely frictional material.

The properties of the interface between the soil and the wall are not easy to identify. Nevertheless, a previous modeling of the plane strain failure of a slope DSRW showed that this property is of secondary importance for triggering failure compared to the brick-to-brick friction and the backfill internal friction angle [11]. The wall-backfill interface (joint) follows also a Mohr-Coulomb law and is addressed the same way as a brick-brick joint. The interface friction angle is unknown in the experiments and we set its value considering the [18]. The relative roughness between the wall and the backfill made of sand [1]. In the case of small clay bricks involved in this work and of the D_{50} of Hostun sand, the asperities can hardly been seen at naked eye and the relative roughness interface is estimated to be of the order of 0.07 - 0.1. Then, this interface cannot be considered as a smooth interface (the normalize roughness should have been smaller than 0.02 [20]) but either as a rough interface as it is the case for actual wall-backfill which relative roughness is greater than 1 [**?**]. Consequently, following the recommendations of the French Regulation for Geotechnical works, the interface friction angle is chosen equal to 2/3 of the backfill internal friction angle which leads to 20° in the case of Hostun sand. This relationship is in accordance with the case of a precast concrete - soil interface. No dilatancy is considered for the wall-backfill interface which is reasonable for an interface composed of a very loose sand. The interface stiffness was estimated considering the coupled system wall-backfill as two springs in series. A normal stiffness of 1×10^9Pa.m^{-1} was then identified for the interface and for the sake of simplicity, the tangential stiffness value was taken equal to the normal stiffness.

The sand-steel block friction angle was taken equal to 16.7° [21]. The Young modulus is equal to 210GPa with a Poisson ratio of 0.27. All the mechanical parameters related to the wall, the backfill and the backfill-wall interface are finally summarized in Table 1.

3.4. Computational aspects

The equilibrium of the unloaded system (without any steel block) under gravity is first computed. In this work, an equilibrium is achieved when the ratio between the unbalanced mechanical force for all gridpoints and the average applied mechanical force magnitude is less than 1×10^{-4}. The unbalanced force vector at a gridpoint is defined at any computation step as the sum of the contact force vectors, the applied force vector and gravity loading.

Additionally, a mechanical damping proportional to the velocity is used. The concept is close to dynamic relaxation [22]: the equations of motion are damped to reach a force

[1]Ratio between the geometrical roughness of the structure $R_{\max}$ to the D_{50} of the soil grains which the diameter of the 50% finer than [19]

equilibrium state as quickly as possible under the applied loading for given boundary conditions. The damping that is used herein, also known as local damping, is defined in such a way that the magnitude of the damping force on a node is proportional to the magnitude of unbalanced forces [23]. A default value of 0.8, recommended for the computations, has been used [22].

For all the simulations performed in this work, the time step for solving the dynamic equations is set to 3×10^{-5}s, value that is smaller than the critical time step.

When building the backfill and searching for the equilibrium of the system, no slippage between bricks was observed within the wall. Moreover, the state of stress within the backfill remained in the elastic domain. Thus, no refined process involving the creation of the backfill in several stages is required.

For the simulation of the backfill loading phases (steel blocks in the experiments), the concentrated loading is imposed in the same manner as for the experiments, increasing the total mass loading a specific area on the backfill surface. More precisely, an incremental mass of 0.1 kg is applied on the backfill surface by increasing the bulk density of the steel block. Each step of loading is applied and the system is let reaching equilibrium before a subsequent loading increment is processed. With this procedure, it is possible to easily identify the force level leading the system to failure. In fact, at failure, the entire system is no more able to balance the applied forces.

Three simulations have been performed. Each one corresponds to one of the three distances between the steel block and the inward wall face (along X-axis), namely 2cm, 3cm or 4cm. Finally, each numerical simulation leading the system to failure took a total time of 2.5 hours on a HP computer of 2.3GHz speed.

4. 3D model validation

4.1. A preliminary result

We give in Fig. 7 a preliminary result corresponding to a distance d between the steel block and the inward wall face of 4cm. In this figure, the evolution of the total force on the backfill is depicted against the horizontal displacement of point D located at wall head. The typical evolution of the loading with respect to the displacements at wall head for slope DSRWs was not obtained (see curve ”no gap” in Fig. 7). Generally, a plateau is clearly noticeable indicating that at a given loading stage, the system cannot withstand further loading. In such a situation, large displacements are generated just before the collapse of the structure [4, 5]. In the performed simulation, this is not the case and the system is capable of mobilizing extra-resistance that allows an indefinite rise of the loading force, which is unrealistic.

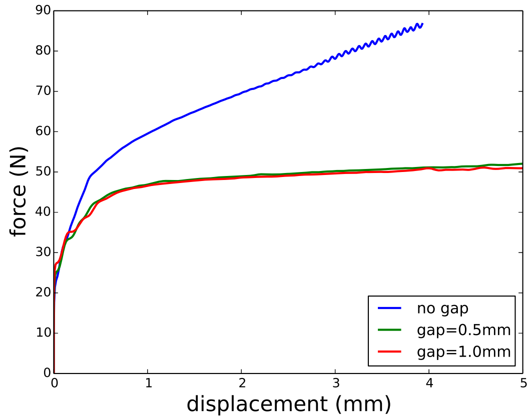

Figure 7: Influence of the gap between bricks on the evolution of the force-displacement curve at point D in the numerical simulations, d = 4cm.

In fact, the method used to create wall bricks by cutting an initial large block, produces perfect face-to-face brick contacts. This perfection is not quite meaningful for an actual brick retaining wall because real clay bricks have not perfect sharp faces with three contact points per face. On the contrary, the irregularities in the vertical faces generate no more than one or two points of contact. In this case, relative displacements and rotations between bricks are easier to occur. This imperfection, present in the actual system, is absent in the proposed DEM modeling. As a result, the perfect contact plane in the DEM modeling generates a strong interlocking between the bricks, inducing jammed states during the loading test. In the simulation, the jammed state is reinforced by the lateral boundary conditions of the wall.

To analyze this effect, the initial configuration which is denoted ”no gap” between bricks, is compared to further computations where a gap of 0.5mm or 1.0mm was inserted between each vertical brick-to-brick contact face (Fig.7). A gap of 0.5mm represents a separation of about 5% of brick thickness, which corresponds to average gaps in an actual dry stone structure [7]. The creation of a gap is made possible by removing some material within the wall and this loss of mass is compensated by increasing the density of the blocks in order to maintain the global wall mass to the former value. We remind here that each brick has a weight of 9.5g.

In Fig. 7, the results show that when the bricks are separated by a gap, the force-displacement curve can reach a steady state which was expected for a valid simulation. Moreover, one can note that increasing the value for the gap does not significantly modify the results. It indicates that if the gap is large enough, the results are no more dependent on its value. In the following, a gap of 0.5mm will be systematically inserted between the vertical planes of contact between bricks in order to let appear a maximum value for the concentrated force.

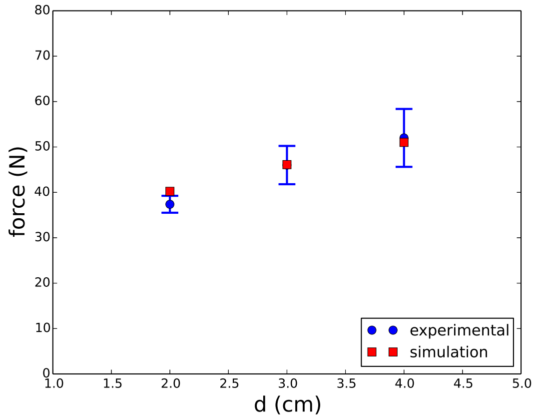

Figure 8: Comparison between the values of force at failure for the experimental tests and numerical simulations for each distance d between the steel block and the inward wall face.

4.2. *Validation of the numerical model*

To validate the numerical model, simulations of the backfill loading with a concentrated force (increasing the mass of a steel box) located at different distances d from the inward wall face were performed. We give in Fig. 8, the values of the concentrated loading F at failure (F_{fail}) for d equal to 2cm, 3cm and 4cm for a Young modulus of 10MPa for the backfill. On this figure, the results obtained through the small-scale experiments are also depicted. One can note that the results from the simulations are in a good agreement with the average values for F found through experiments with d equal to 3cm and 4cm, despite the variability of the experimental results. For d equal to 2cm the result from the simulation is just in a fairly good agreement with the experimental results.

For this distance close to the inward face wall, the limits of the modeling are likely to be highlighted more clearly. We can point out the detachment of the backfill from the wall driven by the movement of elements in the vicinity of the loading block that punches the backfill surface. This feature may only be solved in the numerical model at the expense of a considerable refinement of the mesh which was not attempted herein. The detachment which signifies a deficit of load transfer was also observed for the other simulations with d equal to 3cm or 4cm. Nevertheless, in those cases, the bias was only noticeable for F very close to failure when large displacements were already initiated. In the case of d = 2cm, it takes place for values of F far smaller than F_{fail} and modifies the way the system evolves towards failure. A second argument can be pointed out to explain the apparent strength of the system for d = 2cm. For the sake of simplicity, the elastic properties within the backfill were not taken dependent on depth. Such statement artificially strengthened the soil close to the surface and since in the case of a loading close to the wall it corresponds to the zone that is most loaded, we expect an overestimation of the loading triggering failure.

distance d (cm)	2	3	4
experiments $\overline{F}$ (N)	37.4	46.0	52.0
simulations F (N)	40.2	46.1	51.0
relative error (%)	7.6	0.2	1.9

Table 2: Concentrated loading value F at failure through the experiments and the simulations. $\overline{F}$ denotes the average value for F at failure found through the experiments for a given distance d; E=10MPa.

distance d (cm)	2	3	4
E=5MPa - F_{fail} (N)	44.1	47.1	52.0
E=15MPa - F_{fail} (N)	38.3	44.1	49.1

Table 3: Concentrated loading value F at failure for the numerical simulations, for a backfill Young modulus E equal to 5MPa and 15MPa.

The general results from this study are given in Tab.2. The relative error for the determination of F at failure is found smaller than 8% with respect to the average value $\overline{F}$ throughout the experiments. It can be considered as an encouraging result for a validation of the proposed method for the study of road DSRWs.

Aside to Table 2, we give in Table 3 the maximum loading force obtained for a model where the Young modulus for the backfill was taken equal to 5MPa and 15MPa. Generally, a decrease of the Young modulus is related to an increase of the loading for triggering failure. Indeed, a part of the mechanical work is used to generate irreversible deformations within the backfill, leading to a settlement of the steel block. As a consequence, a smaller part of the loading is transferred to the wall and a larger value for the loading is required for the collapse of the wall.

One can note that the results in Table 3 are within the incertitude inherent to the experiments for d equal to 3cm and 4cm. In the case of d = 2cm, we still observe the shift of the estimate of the force at failure with respect to the experiments. Moreover, in this latter case, the range of values for the force at failure is greater than in the other cases for d. It tends to prove that for d = 2cm, the result is more sensitive to the elastic properties of the backfill.

Finally, given the incertitude of the experiments and the incertitude in the determination of the model parameters, Table 3 tends to comfort the conclusions drawn from Table 2.

4.3. *Failure mode*

As an illustration of the process of deformation of the wall towards failure, the case d = 4cm is studied in more detail in this section.

First, Fig. 9 displays the evolution of the force-displacement curves measured at the four representative points (A,B,C and D) located on the outward wall face. We can note that for a range of F values smaller than a given value that we will

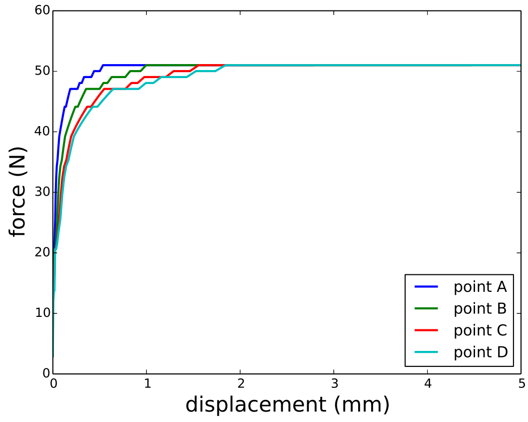

Figure 9: Force-displacement curves for different points of the outward wall face in the numerical simulations; d=4cm.

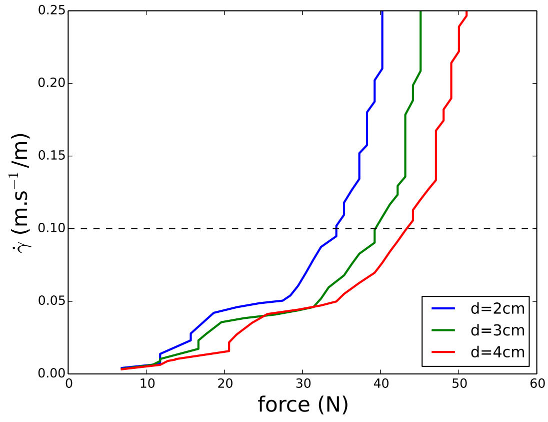

Figure 10: Shear rate as a function of the applied force for point D in the numerical simulations; d=4cm.

denote F_{crit}, the displacements of the bricks are limited. Then, the displacement rate for a given increment of F tends to dramatically increase for subsequent loading stages. In some way, the value of F at this special stage of loading could correspond to a more conventional definition of failure and for this purpose is called critical.

In order to have an estimate of both the force F_{crit} and the associated displacement u_{crit}, the shear rate $\dot{\gamma}$ at point D, which is the point that experienced the greater displacements before failure, was monitored (Fig. 10). The shear rate is obtained as the ratio between the brick velocity measured at point D and the wall height. One can note that when the shear rate exceeds the value of 0.1m.s^{-1}/m, this quantity increases dramatically up to reach the wall collapse. This threshold value (but another value could have been chosen), that was validated for the other studied cases with different values of d, will be chosen for a definition of the critical stage. Knowing the value of F_{crit}, the corresponding u_{crit} value is deduced from Fig. 9. For d = 4cm, F_{crit} is equal to 44.1N (i.e. 86% of the concentrated force on the backfill at failure) while u_{crit} = 0.43mm (0.3% of the wall height).

Fig. 11 displays the evolution of the horizontal displacement of points A, B C and D located on the outward wall face for several stages of loading. At the beginning of the loading stage, the displacements are concentrated at mid-height, creating a bulging profile. This displacement field associated to a small slippage between wall bricks is similar to the iso-stress diagram found under a shallow foundation due to a surface loading in a semi-infinite system (Boussinesq theory). For further force increments, the displacement at a given point more clearly results from a cumulative relative displacements between all bricks located below that point. The profile for F = 45.1N is indicative of the profile obtained for the critical stage (F_{crit} = 44.1N) and the profile for F = 50.1N is indicative of the profile when the system is almost at failure.

Finally, in Fig.11, we can note that the features observed are similar to what was observed throughout full-scale experiments on slope DSRWs [5] where a three-dimensional toppling mode of failure was also observed. Nevertheless, in that case, the failure mode was due to both a concentrated loading on the backfill top surface while a settlement was imposed to the wall foundation which is not the case herein.

Fig. 12 gives the horizontal stress field while the concentrated load increases on the backfill surface (the wall which should appear on the left side of the system was removed). On this figure, negative stresses denote compressive stresses. One can note that the contour of iso-stresses roughly follows the distribution predicted by the Boussinesq theory (but here some degree of plasticity exists) and as a result, the maximum stresses on the wall are found in a zone at wall mid-height. It means that, at this loading stage and before subsequent loading increments, the horizontal displacements affect preferentially the zones where point B and C are located.

When the loading increases, the stress distribution evolves and plasticity within the soil develops upward and downward from this previously mentioned mid-height zone. Nevertheless, the development of extra stresses is more intense upward (Fig.12c and Fig.12d). It may due to the close bottom boundary that disturbs the distribution of stresses. It implies that subsequent loading increments will have a more important impact on the upper mid-height zone (points C and D) than those located below (points A and B). It explains the displacements profile at the stage where F is equal to 45.1N (Fig.11). Furthermore, a larger increase of the horizontal stresses upward facilitates the increase of driving forces triggering a possible failure (case for example of a toppling mode of failure).

We give in Fig.13, a sketch of the plasticity state of elements within the backfill just before failure. One can note that a large

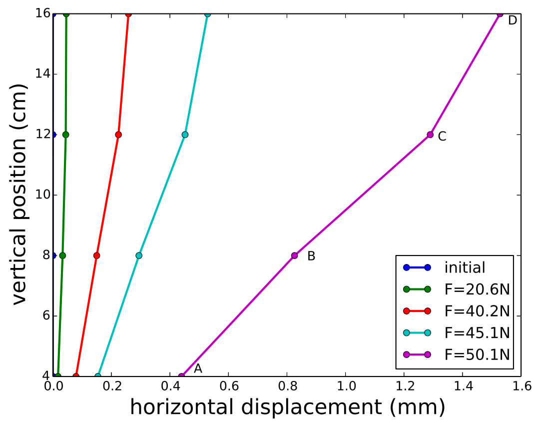

Figure 11: Horizontal displacements of points A, B, C and D as a function of loading F in the numerical simulations; d=4cm.

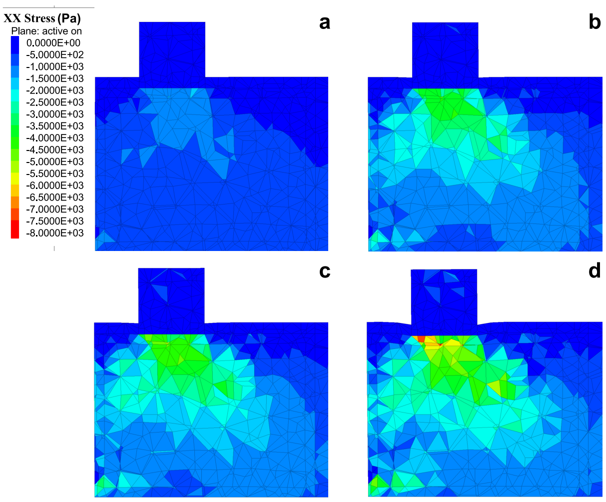

Figure 12: Horizontal stress field (σ_{XX}) in the backfill as a function of the applied load for $d = 4cm$: a) F=20.6N; b) F=40.2N; c) F=45.1N; d) F=50.0N.

zone surrounding the steel block and involving the whole wall lengthwise has reached the Mohr-Coulomb criterion when failure is triggered. For $d = 4$cm, failure is then monitored by the backfill internal friction angle and in a lesser extent by the elastic properties of the backfill. It tends to limit for that d value the possible error in the choice of the elastic properties of the backfill on the behavior of the system.

We display in Fig. 14a, the displacement field of the whole system for F equal to 51N, which is the force value at failure. On this figure, we can define what can be denoted the maximum length of influence of the loading l_i on the brick wall. It defines the extent of the zone of the wall where repair will be required in case of failure. We consider that the displacement of the bricks due to the concentrated loading is insignificant when the ratio between the total horizontal displacement of a brick and the wall thickness (i.e. 33mm) is smaller than

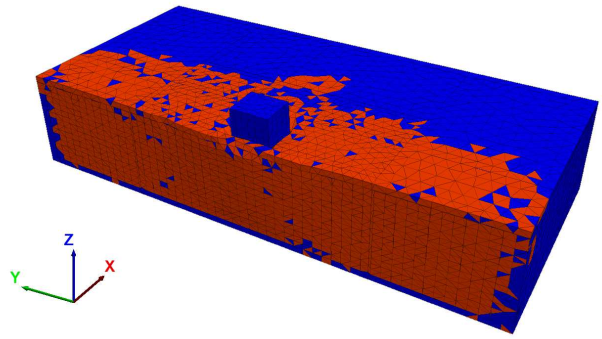

Figure 13: Focus on the backfill elements which reached the plasticity state for $F = F_{\text{fail}}$. Here, these elements are tainted red.

1%. Here, this length of influence, measured at wall head, is approximately equal to 67cm which is close to 68cm that was found in the experiments (Fig. 4). This length is expected to depend on the width of the steel block parallel to the face wall, on the distance d but also on the properties of the backfill. It may also depend on other factors such as, bricks arrangement and bricks geometry [11]. One can note that this distance is smaller than the wall length (lengthwise) which proves that the lateral boundary conditions do not interfere with the wall failure.

Fig. 14b depicts the total displacements within the cross-sectional plane of symmetry of the whole system including points A, B, C and D for F equal to 51N. The zone affected by the surface loading is clear on this sketch which also evidences the shape of the failure surface within the backfill. This surface crosses the wall at the foot of the wall, certainly guided by the fixed first row of bricks.

In this cross-section, failure is achieved by a mode similar to a toppling mode, where the second layer of bricks still fixed and where the other upper bricks move outward following an overturning motion as a monolithic assembly. The rotation of bricks produces the separation between the bricks of the inward wall face and those from the outward wall face (Fig. 14b). This separation is initiated when the displacement u at wall head reaches approximatively u_{crit}.

4.4. *Influence of the distance of loading from the inward wall face*

Section 4.2 evidenced that the value of the concentrated loading F at failure depends on the distance d between the steel box and the inward wall face. This result is also emphasized in Fig.15 where the evolution of the force-displacement curves for point D with d equal to 2cm, 3cm and 4cm are depicted.

This holds true for the other computed characteristics of the system. For example, the critical value for the concentrated force F_{crit}, below which few displacements are generated,

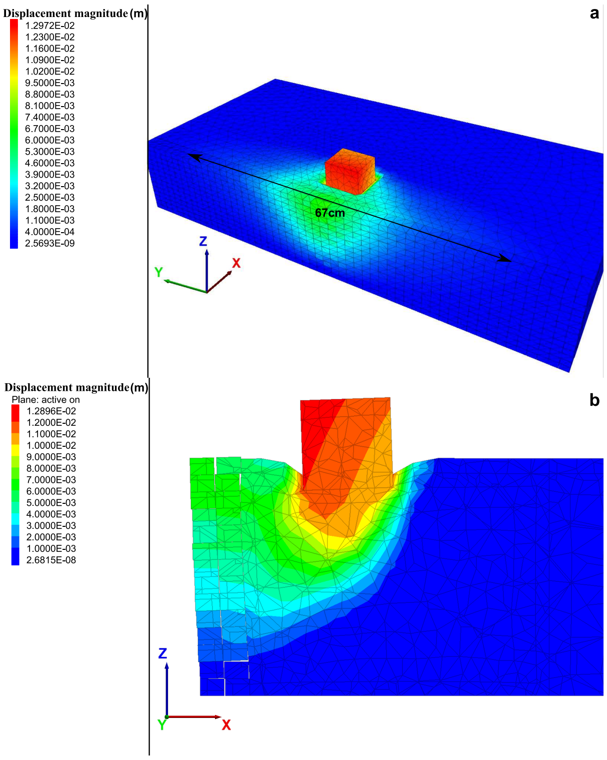

Figure 14: Displacement magnitude just before failure; $d = 4$cm: (a) Whole system. (b) Cross-sectional plane of symmetry.

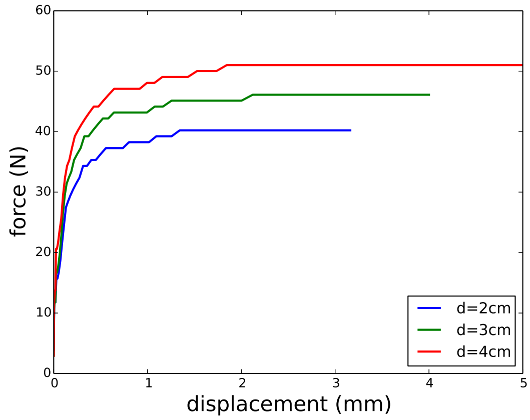

Figure 15: Force-displacement curves as a function of the distance d between the loading steel block and the wall inward face. Displacements are measured at wall head (point D).

distance d (cm)	2	3	4
F_{crit} (N)	34.3	39.2	44.1
u_{crit} (mm)	0.31	0.33	0.43
F_{fail} (N)	40.2	46.1	51.0
l_i (cm)	58	63	67

Table 4: Evolution of some characteristics at point D with the distance d; E=10MPa.

also differs according to d. In section 4.3, we mentioned that for $d = 4$cm, this value corresponded to 86% of F_{fail}. For $d = 3$cm, F_{crit} corresponds to 85% of F_{fail} and for $d = 2$cm, F_{crit} corresponds to 84% of F_{fail}. These percentages, though very close to each other, increase as a function of the distance between the wall and the loading block. It indicates that when the loading block is far to the wall, failure takes place more like in an unstable system (F_{crit} and F_{fail} are quite similar in that case). As a conclusion, for the studied system, the simulations showed that for F lower than $F_{\mathrm{crit}} \simeq 0.8F_{\mathrm{fail}}$, few displacements are expected at point D. Thus, below this critical value, the wall is not expected to experience significant movements. F_{crit} values and associated displacements u_{crit} for any d distances are given in Table 4.

As a correspondence, we give in this table for each distance d the maximum length of influence l_i (measured at wall head and lengthwise) of the concentrated loading. As expected, the length of influence of the loading increases as a function of the distance d. As the distance d increases, a given iso-stress diagram intercept a larger zone of the wall. The difference between the smallest and the largest value for l_i corresponds to three brick lengths which is not negligible at the scale of the system.

Fig. 16a and Fig. 16b displays the horizontal stress field (σ_{XX}) for a distance between the loading block and the inward wall face for $d = 2$cm and $d = 4$cm respectively, just before the wall collapse (the wall which should appear on the left side of the systems was removed). For the case when the loading block is close to the inward wall face, the horizontal stress field concentrates in the upper wall mid-height (Fig.16a). On the contrary, when the block is at 4cm from the inward wall face, these stresses concentrate more in a lower central zone of the wall which contributes to the wall disequilibrium in a lesser extent (Fig.16b). Thus, a larger force on the backfill is required to induce the wall failure.

4.5. Influence of the backfill Young modulus

In order to complement the study and to take into account of a possible uncorrect calibration of the backfill Young modulus, we give in Tables 5 and 6 some characteristics of the system towards failure for $E = 5$MPa and $E = 15$MPa respectively.

As pointed out in sections 4.2 and 4.3, the tendency is to an increase of the concentrated force at failure F_{fail}, irrespective of d, when the Young modulus decreases. It also holds true for F_{crit}. The reason for this trends cannot be found in the different values of the backfill punching of the steel box for different Young modulus values. In fact, the settlement of the steel box when F_{fail} is reached (beginning of the plateaus in Fig. 15) is of the order of 3-4mm which is not significant compared to the backfill height (160mm).

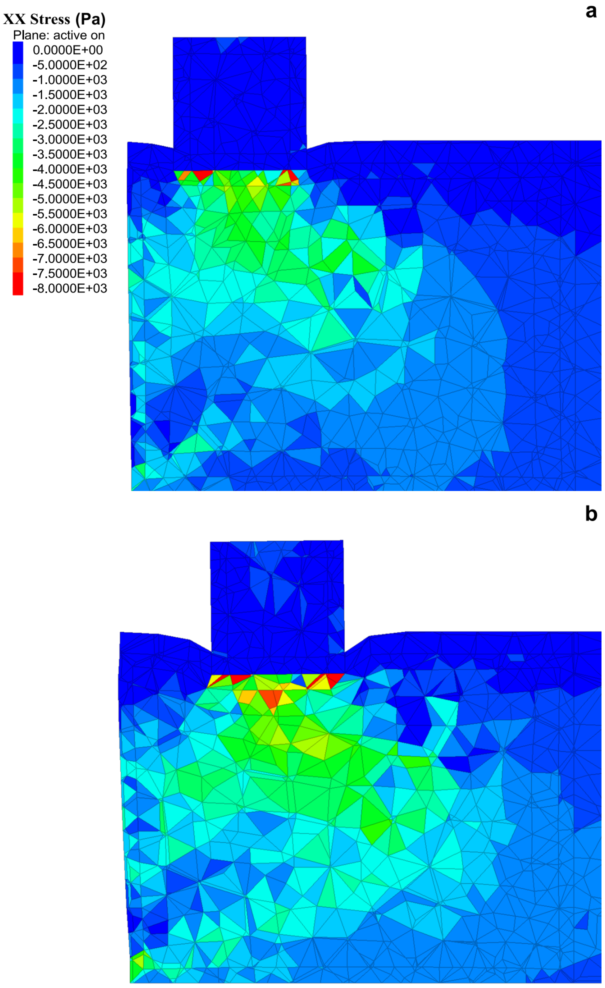

Figure 16: Horizontal stress field (σ_{XX}) as a function of the distance wall-loading block, for the final stage of loading: a) d = 2cm. b) d = 4cm.

Some studies about soil- structure interaction showed that the mechanical influence of the soil on a structure (hence of the backfill on the wall) is rather similar to the action of a normal spring with a given stiffness [24] and hence is not equivalent to a condition of constant normal load. While the backfill behavior is elastic, this stiffness is directly related to the Young modulus. Consequently, the intensity of transfer of loading from the wall to the backfill decreases as the Young modulus decreases. It means it will require a higher value for F_{fail} to induce the wall failure, which is what was obtained through the simulations. Moreover, in this system, we observed that plasticity was created for values of F smaller than $F_{\text{fail}}/10$. Consequently, a large part of the backfill loading with the concentrated loading takes place while the soil is in the plastic domain. Fore example, Fig. 13 depicts the plastified domain when F_{fail} is reached. The nature of plasticity is to relax stresses by creating plastic deformations which tends to decrease the apparent stiffness of the backfill. Then the possibility for plasticity intensifies the decrease of the loading transfer to the wall while the Young modulus decreases.

distance d (cm)	2	3	4
F_{crit} (N)	38.2	43.2	49.1
u_{crit} (mm)	0.16	0.24	0.27
F_{fail} (N)	44.1	47.1	52.0
l_i (cm)	56	59	60

Table 5: Evolution of some characteristics with the distance d for E=5MPa.

distance d (cm)	2	3	4
F_{crit} (N)	32.4	39.2	42.2
u_{crit} (mm)	0.28	0.38	0.40
F_{fail} (N)	38.3	44.1	49.1
l_i (cm)	61	63	67

Table 6: Evolution of some characteristics with the distance d for E=15MPa.

Concerning the tendencies for u_{crit}, it seems difficult to conduct a deep analysis of involved phenomena. Actually, in DEM computations, the system is very often subject to local blockages that are destroyed by subsequent loading increments. Then, at a given stage of the loading, the displacements at point D may not be strictly representative and general trends may be hidden. For example, we observed the same trends for u_{crit} for d equal to 3cm and 4cm while the results obtained for d equal to 2cm does not match this trend.

5. Conclusion

In this paper, 3D DEM simulations to study the failure of a scale-down road dry stone retaining wall were presented. These simulations model an experimental campaign where a concentrated loading represented by superposed steel blocks was placed at the backfill surface. Different distances between the steel block and the inward wall face were investigated. For each distance, five different tests leading to failure have been performed.

The DEM modeling of the three-dimensional DSRW failure involved a discrete modeling of the wall by individual blocks and a continuum modeling of the backfill while the backfill-wall joint is ruled by a homogenized law. To correctly retrieve the features observed through the small-scale experiments, a certain micro-gap between the vertical joints of the wall bricks was introduced. It avoids the existence of jammed states and though artificial, may be interpreted as a necessary factor of imperfection inherent to actual systems that needs to be included in any simulation of 3D DSRWs. The minimum value stabilizing the simulation is given.

In a first stage of loading, the loading generates a small bulging at wall mid-height, then the increase of stresses on the wall radiates both downward and upward. Nevertheless, the increase of stresses upward is found more intense in the upper mid-part of the wall. As a result, a toppling mode of failure is obtained. The impact of the failure on the wall-lengthwise is limited, similar to what is observed through the experiments.

The distance between the concentrated loading and the inward wall face influences the value of the force at failure. It is mainly due to a distribution of horizontal stresses which is more critical for the wall stability when the concentrated loading is closer to the wall. Indeed, it directly affects the upper part of the wall increasing in a more easy way the driving overturning forces towards failure. This result was nevertheless expected. Finally, the influence length of the loading which gives the possible extent zone of damage in the wall seems dependent on this distance.

The concentrated force values leading to failure in the simulations are found in a good agreement with the average force values obtained throughout the experiments except for the case when the loading is very close to the wall for which the relative error reached 8%. The detachment of the backfill from the wall at wall head may explain this departure. Moreover, in the case where the loading is very close to the wall, the limits of a continuum approach for the backfill that cannot properly model features have been reached due the large distortions that took place.

The incertitude of results in relation to the backfill Young modulus was estimated. A decrease of a Young modulus increasing the dissipation of energy by the generation of irreversible deformations, allowed for the concentrated force to increase. The same trend is observed for the critical value of the concentrated force below which few displacements are induced by the loading. In general, the incertitude related to the identification of the Young modulus remained within the range of incertitude of the experiments. It is not the case when the concentrated loading is very close to the wall where the system seems more sensitive to a change of the backfill Young modulus.

In conclusion, this work can be considered as encouraging for the validation of the mixed discrete-continuum approach as a possible technique for the study of the behavior of road DSRWs. Nevertheless, at this stage, it is too early to extrapolate the results of this study to actual systems. In an actual DSRW, the wall thickness allows a more sophisticated arrangement of blocks. Moreover, actual blocks are more irregularly shaped than in this study. Nevertheless, the main features observed in this study are expected to occur on site for actual DSRWs.

6. Notations

d	distance between the steel block (concentrated loading) and the inward wall face
F	value of the concentrated force acting on the backfill surface
$\overline{F}$	average value of the concentrated force F at failure found through experiments for a given distance d
F_{fail}	value of the concentrated F force at failure through the simulation for a given distance d
F_{crit}	critical value for F above which a small increase of F generates large displacements
u_{crit}	horizontal displacement at wall head associated to F_{crit}
l_i	influence length of the concentrated loading measured at wall head (lengthwise)

7. Acknowledgments

The present work is part of the research project MapCoD (Materials and processes for sustainable constructions) and was financially supported by the program Projet d'Avenir Lyon-Saint Etienne of University of Lyon which is part of the program "Investments for the Future" ANR-11-IDEX-0007 (National Agency of Research). The authors want to acknowledge these institutions for their support and would like also to thank Kimberly Morin-Coulomb, Stéphane Cointet and Laureen Giraud for performing the experimental tests.

References

[1] A. Colas, J. Morel, D. Garnier, Yield design of dry-stone masonry retaining structurescomparisons with analytical, numerical, and experimental data, International journal for numerical and analytical methods in geomechanics 32 (2008) 1817–1832.

[2] J. Burgoyne, Revetments or retaining walls, Corps of royal engineers 3 (1853) 154–159.

[3] B. Villemus, J. Morel, C. Boutin, Experimental assessment of dry stone retaining wall stability on a rigid foundation, Engineering structures 29 (2007) 2124–2132.

[4] A. S. Colas, J. C. Morel, D. Garnier, Full-scale field trials to assess dry-stone retaining wall stability, Engineering Structures 32 (2010) 1215–1222.

[5] C. Mundell, P. F. McCombie, A. Heath, J. Harkness, P. Walker, Behaviour of drystone retaining structures, Proceedings of the Institution of Civil Engineers-Structures and Buildings 163 (2010) 3–12.

[6] X. Zhang, N. Koutsabeloulis, S. Hope, A. Pearce, A finite element analysis for the stability of drystone masonry retaining walls, Géotechnique 54 (2004).

[7] R. Harkness, W. Powrie, X. Zhang, K. Brady, M. O'Reilly, Numerical modelling of full-scale tests on drystone masonry retaining walls, Geotechnique 50 (2000) 165–179.

[8] Itasca Consulting Group Inc., Universal Distinct Element Code 5UDEC) Version 2.0: user's manual., Minneapolis, Minnesota, 2th edition, 1993.

[9] W. Powrie, R. Harkness, X. Zhang, D. Bush, Deformation and failure modes of drystone retaining walls, Geotechnique 52 (2002) 435–446.

[10] M. Claxton, R. A. Hart, P. F. McCombie, P. J. Walker, Rigid block distinct-element modeling of dry-stone retaining walls in plane strain, Journal of geotechnical and geoenvironmental engineering 131 (2005) 381–389.

[11] J. J. Oetomo, E. Vincens, F. Dedecker, J. C. Morel, Modeling the 2d behavior of drystone retaining walls by a fully discrete element method, Int. J. Numer. Anal. Meth. Geomech. DOI: 10.1002/nag.2480 (2015). (In Press).

[12] E. Flavigny, J. Desrues, B. Palayer, Note technique-le sable d'hostun" rf", Revue française de géotechnique (1990) 67–70.
[13] Itasca Consulting Group Inc., 3 Dimensional Distinct Element Code. Theory and Background., Minneapolis, Minnesota, 4th edition, 2013.
[14] P. Walker, P. McCombie, M. Claxton, Plane strain numerical model for drystone retaining walls, Proceedings of the ICE-Geotechnical Engineering 160 (2007) 97–103.
[15] J. Biarez, P.-Y. Hicher, et al., Elementary mechanics of soil behaviour: saturated remoulded soils., AA Balkema, 1994.
[16] T. Iwasaki, F. Tatsuoka, Effects of grain size and grading on dynamic shear moduli of sands, Soils and foundations (1977).
[17] C. Dano, P.-Y. Hicher, Evolution of elastic shear modulus in granular materials along isotropic and deviatoric stress paths, in: 15th ASCE Engineering Mechanics Conference.
[18] R. Frank, Eurocode 7 on geotechnical design: a code for soil-structure interaction, eurocode 7 calcul géotechnique: un code pour l'interaction sol-structure, J. Appl. Eng. Sci. Technol (2014) 1–10.
[19] H. Kishida, M. Uesugi, Tests of the interface between sand and steel in the simple shear apparatus, Géotechnique 37 (1987) 45–52.
[20] V. Fioravante, On the shaft friction modelling of non-displacement piles in sands, Soils and Foundations 42 (2002) 23–33.
[21] E. Rabinowicz, Friction and Wear of Materials, Wiley, New York, 1965.
[22] J. R. H. Otter, A. C. Cassell, R. E. Hobbs, et al., Dynamic relaxation, in: ICE proceedings, 4, Thomas Telford, pp. 633–656.
[23] P. Cundall, Distinct element models of rock and soil structure, Analytical and computational methods in engineering rock mechanics 4 (1987) 129–163.
[24] M. Boulon, Basic features of soil structure interface behaviour, Computers and Geotechnics 7 (1989) 115–131.